Journal of Computational Physics **179,** 649–664 (2002)
doi:10.1006/jcph.2002.7081

Comparison of Numerical Schemes for the Solution of the Ice-Thickness Equation in a Dynamic/Thermodynamic Ice-Sheet Model

Ralf Greve* and Reinhard Calov†

**Fachbereich Mechanik, Technische Universität Darmstadt, Hochschulstrasse 1, D-64289 Darmstadt, Germany; and †Potsdam-Institut für Klimafolgenforschung, Postfach 601203, D-14412 Potsdam, Germany*
E-mail: greve@mechanik.tu-darmstadt.de

Received September 18, 2001; revised April 8, 2002

A general finite-difference marching scheme for the numerical solution of the ice-thickness equation in ice sheets is considered. From this scheme, a variety of explicit, ADI, implicit and over-implicit methods can be derived. These methods are compared for stability and accuracy within the dynamic/thermodynamic ice-sheet model SICOPOLIS for two different problems: (i) a simple axi-symmetric steady-state ice sheet which rests on a flat bedrock, and (ii) the time-dependent paleo-glaciation of the northern hemisphere. As expected, over-implicit methods turn out to be most stable. For the simple problem, all schemes provide a good accuracy, whereas for the northern hemisphere simulations, the accuracy of the over-implicit scheme is not satisfactory, so that the implicit technique without over-weighing appears favorable for this application.

Key Words: finite-difference methods; applications to physics; Stokes and related flows; computational methods; glaciology.

1. INTRODUCTION

Ice sheets are extended ice masses which rest on solid land and have been formed by accumulated snowfall over thousands of years. At present, two large ice sheets exist on Earth, the Antarctic and the Greenland ice sheets, which store about 90% of the entire available freshwater. In case of total disintegration, global sea level would rise by approximately 70 meters. In the past, the Earth experienced periods with a much more pronounced glaciation. Twenty one thousand years ago, at the Last Glacial Maximum, ice sheets covered also large parts of North America, the European Alps, the northern part of Europe and perhaps Siberia and Tibet, and consequently the sea level was ca. 130 meters lower than today [5].

On time scales of centuries and more, ice sheets represent an important dynamic part of the climate system. This is so because ice flows under its own weight, so that a balance

0021-9991/02 $35.00

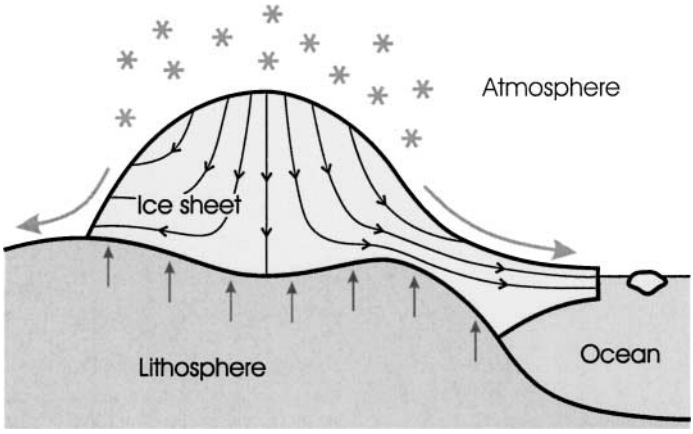

FIG. 1. Flowing ice sheet with attached, floating ice shelf, and its interaction with the atmosphere, the ocean and the lithosphere due to topography, snowfall, melting, calving, and geothermal heat flux.

between snowfall (accumulation) in the interior, melting (ablation) and calving close to the margin, and ice flow from the interior toward the margin occurs. Due to the strong dependence of ice viscosity on temperature, thermodynamic effects come further into play. The situation is illustrated in Fig. 1.

Several models have been developed to simulate different aspects of ice-sheet dynamics like present states of Antarctica, Greenland and smaller ice caps, reconstructions of paleo-glaciation and retreat scenarios under increasing greenhouse-gas concentrations in the atmosphere (for an overview of relevant literature, see [2, 3, 14, 18]). Typically, in such models, the central evolution equation is the one for the ice thickness, which describes the changes of the ice thickness and extent over time. In this paper, after outlining the underlying continuum-mechanical and thermodynamical theory and numerical solution strategy of the ice-sheet model SICOPOLIS (Section 2), a general finite-difference marching scheme for the ice-thickness equation is considered, from which several explicit and implicit methods can be derived, including the over-implicit scheme recently proposed by Hindmarsh [10]. This scheme was proven to be unconditionally stable for the special case of an isothermal ice sheet under certain conditions (Section 3). These methods will be compared for stability and accuracy within the model SICOPOLIS for a simple, "academic" steady-state problem (Section 4) as well as for time-dependent paleoclimatic simulations of northern-hemisphere glaciation (Section 5). The main findings are summarized in the conclusions (Section 6).

2. DYNAMIC/THERMODYNAMIC ICE-SHEET MODEL

The mathematical model used here in order to describe the dynamics and thermodynamics of ice sheets is that described by Greve [6, 7]. It is based on the continuum-mechanical balance equations and jump conditions of mass, momentum and energy, and the rheology of a density-preserving, heat-conducting power-law fluid with a rate factor strongly dependent on the temperature T and the water content ω,

$$\boldsymbol{D} = EA(T', \omega)\, f(\sigma)\, \boldsymbol{t}^{\mathrm{D}}, \tag{1}$$

where $\boldsymbol{D}$ is the strain-rate tensor; $\boldsymbol{t}^{\mathrm{D}}$ the stress deviator; E the creep enhancement factor; $A(T', \omega)$ the creep rate factor, dependent on the homologous temperature $T' = T - T_{\mathrm{m}}$ (T_{m}: pressure melting point) and the water content ω (the latter holds only in temperate ice, that is, at pressure melting $T' = 0°\mathrm{C}$); $f(\sigma)$ the creep function, dependent on the effective shear stress $\sigma = [\mathrm{tr}(\boldsymbol{t}^{\mathrm{D}})^2/2]^{1/2}$. For the creep function, we apply the widely used power-law

$$f(\sigma) = \sigma^{n-1}, \quad \text{with power-law exponent } n = 3, \tag{2}$$

which is known as Glen's flow law (e.g., [17]).

The model equations, which shall not be repeated here except for the ice-thickness equation that is the subject of this study, are subjected to the shallow ice approximation [12, 16]; that is, they are scaled with respect to the aspect ratio $\varepsilon \sim 10^{-2} \ldots 10^{-3}$ (ratio of typical thickness to typical horizontal extent), and only lowest-order terms are kept. This entails neglection of acceleration in the momentum balance, so that the velocity field behaves quasi-stationary ("Stokes flow") and, furthermore, neglection of deviatoric normal stresses.

The evolution equation for the ice thickness is based on the incompressibility condition

$$\nabla \cdot \boldsymbol{v} = \frac{\partial v_x}{\partial x} + \frac{\partial v_y}{\partial y} + \frac{\partial v_z}{\partial z} = 0, \tag{3}$$

where x, y are the horizontal Cartesian coordinates, z is the vertical Cartesian coordinate (elevation above present sea level), and $\boldsymbol{v} = (v_x,\ v_y,\ v_z)$ the three-dimensional ice-velocity vector. Integration of (3) from the ice surface, $z = h(x, y, t)$, to the ice base, $z = b(x, y, t)$, and application of kinematic boundary conditions at the surface and the base yields

$$\frac{\partial h}{\partial t} = -\frac{\partial q_x}{\partial x} - \frac{\partial q_y}{\partial y} + a_{\mathrm{s}} - a_{\mathrm{b}} + \frac{\partial b}{\partial t}, \tag{4}$$

where t is the time,

$$\boldsymbol{q} = (q_x,\ q_y) = \int_b^h (v_x,\ v_y)\, dz \tag{5}$$

the horizontal mass flux, $a_{\mathrm{s}}(x, y, t)$ the accumulation-ablation function at the ice surface (accumulation, a_{s}^+, minus ablation, a_{s}^-) and $a_{\mathrm{b}}(x, y, t)$ the basal melting rate. In the shallow-ice approximation, the horizontal mass flux can be expressed as

$$(q_x,\ q_y) = -D_{\mathrm{h}}\left(\frac{\partial h}{\partial x},\ \frac{\partial h}{\partial y}\right), \tag{6}$$

with the diffusivity

$$\begin{aligned} D_{\mathrm{h}} &= \rho g H^2 C(T', \ldots) + 2\rho g \int_b^h EA(T', \omega) f(\sigma)\, (h - z)^2\, dz \\ &= \rho g H^2 C(T', \ldots) + 2(\rho g)^n \left(\left(\frac{\partial h}{\partial x}\right)^2 + \left(\frac{\partial h}{\partial y}\right)^2 \right)^{\frac{n-1}{2}} \int_b^h EA(T', \omega)(h - z)^{n+1}\, dz, \end{aligned} \tag{7}$$

where ρ is the ice density, g the gravity acceleration, and $H = h - b$ the ice thickness (e.g., [13]; the second form follows from the first by applying Eq. (2)). $C(T', \ldots)$ denotes the coefficient in the Weertman-type basal-sliding law

$$\left(v_x^{\mathrm{b}},\ v_y^{\mathrm{b}}\right) = C(T', \ldots)\left(\tau_{xz}^{\mathrm{b}}, \tau_{yz}^{\mathrm{b}}\right), \tag{8}$$

which relates the velocity at the ice base, $(v_x^{\mathrm{b}},\ v_y^{\mathrm{b}})$, to the basal shear stress $(\tau_{xz}^{\mathrm{b}},\ \tau_{yz}^{\mathrm{b}})$. $C(T', \ldots)$ depends on the homologous temperature, T', and perhaps other quantities such as the pressure and the absolute value of the basal shear stress.

Insertion of (6) into (4) yields the evolution equation for the ice thickness $H = h - b$,

$$\frac{\partial h}{\partial t} = \frac{\partial}{\partial x}\left(D_{\mathrm{h}}\frac{\partial h}{\partial x}\right) + \frac{\partial}{\partial y}\left(D_{\mathrm{h}}\frac{\partial h}{\partial y}\right) + a_{\mathrm{s}} - a_{\mathrm{b}} + \frac{\partial b}{\partial t}, \tag{9}$$

(which is actually an evolution equation for the free surface, h, but in agreement with the common terminology referred to as "ice-thickness equation"). Note that, according to (7), D_{h} depends itself on h, so that (9) is a nonlinear partial differential equation of parabolic type.

To solve the complete set of model equations, the numerical model SICOPOLIS (Simulation Code for Polythermal Ice Sheets) was developed. It is based on a finite-difference approach with discretizations

$$x_i = x_0 + i\Delta x, \quad i = 0\,(1)\,i_{\max}, \tag{10}$$

$$y_j = y_0 + j\Delta y, \quad j = 0\,(1)\,j_{\max}, \tag{11}$$

$$t^n = t^0 + n\Delta t, \quad n = 0\,(1)\,n_{\max} \tag{12}$$

[the notation $a\ (b)\ c$ means "from a to c in steps of b"]. In the vertical direction (coordinate z), columns of cold ice, temperate ice and lithosphere are mapped separately on intervals $\zeta = 0 \ldots 1$ ("σ-transformation"), and the coordinates ζ are discretized in a fashion analogous

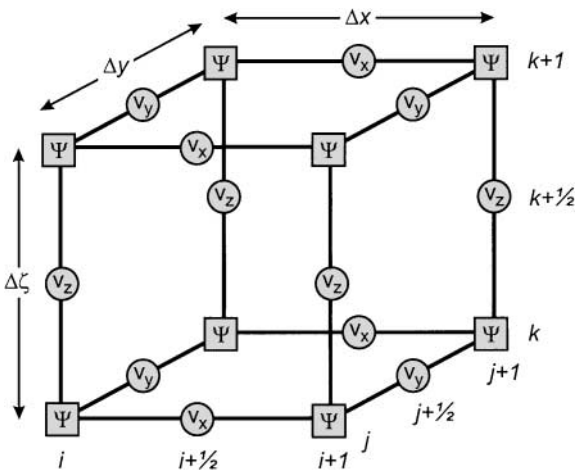

FIG. 2. Arakawa-C-grid applied in the ice-sheet model SICOPOLIS. Velocity components v_x, v_y, v_z are defined in between grid points, other variables Ψ (temperature, water content, positions of free surface and bedrock, etc.) are defined on grid points.

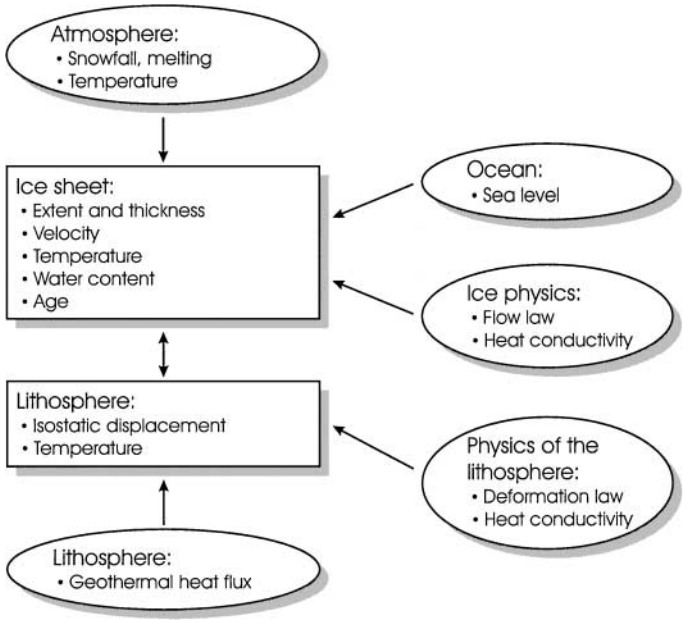

FIG. 3. Scheme of the polythermal ice-sheet model SICOPOLIS. The rectangular boxes correspond to prognostic model components, the oval boxes to input quantities.

to (10)–(12). Variables are distributed on the numerical grid according to the Arakawa-C-scheme [1], which means that velocity components v_x, v_y, and v_z are defined in between grid points, whereas the ice surface h and other variables are taken on grid points (Fig. 2). Arakawa and Lamb [1] reported that this scheme is best suited for simulating the geostrophic adjustment for the shallow-water equations, a problem very similar to the flow of ice sheets. For that reason, the Arakawa-C-grid is used in most of the current ice-sheet models based on finite differences.

Two different time steps apply, a smaller one, Δt, for the solution of the ice-thickness equation (9), together with the evolution equation for the bedrock position b, and a larger one, $\widetilde{\Delta t}$, for the thermodynamic evolution equations (temperature in cold ice, water content in temperate ice, age). It is required that $\widetilde{\Delta t}$ is an integer multiple of Δt.

The model computes three-dimensionally the temporal evolution of ice extent, thickness, isostatic lithosphere displacement, ice velocity (purely diagnostic equation), temperature, water content, and age as a response to external forcing. The latter must be specified by (i) the mean annual air temperature above the ice, (ii) the surface mass balance, which is ice accumulation (snowfall) minus ablation (melting), (iii) the eustatic sea level, and (iv) the geothermal heat flux, imposed 5 km below the ice-bedrock interface in order to account for thermal inertia effects of the lithosphere. The model is sketched schematically in Fig. 3. For further details, see Greve [6, 8].

3. NUMERICAL SOLUTION OF THE ICE-THICKNESS EQUATION

Let us now turn to the numerical solution of the diffusive ice-thickness equation (9). We define the forward-time operator

$$(\delta_t h)^n_{i,j} = \frac{h^{n+1}_{i,j} - h^n_{i,j}}{\Delta t} \tag{13}$$

and the central-space operators

$$\left(\delta_x^2 h\right)_{i,j}^{n(+1)} = \frac{1}{\Delta x^2}\left((D_\mathrm{h})_{i+\frac{1}{2},j}^{n}\left(h_{i+1,j}^{n(+1)} - h_{i,j}^{n(+1)}\right) - (D_\mathrm{h})_{i-\frac{1}{2},j}^{n}\left(h_{i,j}^{n(+1)} - h_{i-1,j}^{n(+1)}\right)\right), \quad (14)$$

$$\left(\delta_y^2 h\right)_{i,j}^{n(+1)} = \frac{1}{\Delta y^2}\left((D_\mathrm{h})_{i,j+\frac{1}{2}}^{n}\left(h_{i,j+1}^{n(+1)} - h_{i,j}^{n(+1)}\right) - (D_\mathrm{h})_{i,j-\frac{1}{2}}^{n}\left(h_{i,j}^{n(+1)} - h_{i,j-1}^{n(+1)}\right)\right) \quad (15)$$

(due to the spatially varying diffusivity D_h, this is not simply the discretization of second spatial derivatives of h), in which the diffusivities are always taken at the old time level t^n, and are evaluated as

$$(D_\mathrm{h})_{i\pm\frac{1}{2},j}^{n} = \frac{1}{2}\left((D_\mathrm{h})_{i,j}^{n} + (D_\mathrm{h})_{i\pm1,j}^{n}\right), \quad (16)$$

$$(D_\mathrm{h})_{i,j\pm\frac{1}{2}}^{n} = \frac{1}{2}\left((D_\mathrm{h})_{i,j}^{n} + (D_\mathrm{h})_{i,j\pm1}^{n}\right). \quad (17)$$

Equations (16) and (17) correspond to the "Type II" method described by Huybrechts *et al.* [14], which is characterized by favorable stability properties. A finite-difference marching scheme of the general form

$$\begin{aligned}(\delta_t h)_{i,j}^{n} = {} & w_x\left(\delta_x^2 h\right)_{i,j}^{n+1} + (1-w_x)\left(\delta_x^2 h\right)_{i,j}^{n} + w_y\left(\delta_y^2 h\right)_{i,j}^{n+1} + (1-w_y)\left(\delta_y^2 h\right)_{i,j}^{n} \\ & + (a_\mathrm{s})_{i,j}^{n} - (a_\mathrm{b})_{i,j}^{n} + \left(\frac{\partial b}{\partial t}\right)_{i,j}^{n}\end{aligned} \quad (18)$$

is considered, which holds for $i = 1\,(1)\,i_\mathrm{max} - 1$, $j = 1\,(1)\,j_\mathrm{max} - 1$, $n = 0\,(1)\,n_\mathrm{max} - 1$. For the initial time level $n = 0$ and the boundaries $i = 0,\ i_\mathrm{max}$ and $j = 0,\ j_\mathrm{max}$, the surface elevations $h_{i,j}^{n}$ are prescribed.

For $w_x = w_y =: w = 0$ the scheme (18) is explicit (EXPL), and an alternating choice $w_x = 0$, $w_y = 1$ in one iteration step and $w_x = 1$, $w_y = 0$ in the next yields an alternating-direction implicit scheme (ADI). Most of the current ice-sheet models (see [14, 18]) use one of these two easy-to-implement and well-tried methods. For $w_x = w_y =: w = 1$, the scheme becomes implicit (IMPL), for $w_x = w_y =: w = 1/2$ it is of Crank–Nicholson type (will not be discussed further). Hindmarsh [10] proposed an over-implicit scheme (OVI) with $w_x = w_y =: w > 1$, and proved its unconditional stability in case of an isothermal ice sheet for $w \geq n/2$. We will also consider a combination of ADI and OVI, that is, $w_x = 0$, $w_y =: w > 1$ in one iteration step and $w_x =: w > 1$, $w_y = 0$ in the next (alternating-direction over-implicit, ADOVI). All schemes are implemented as options in the latest version of SICOPOLIS.

In case of the explicit scheme, (18) can be solved directly for the unknowns $h_{i,j}^{n+1}$. In all other cases, systems of linear equations (SLEs) arise from (18). For the moment, let us assume a quadratic horizontal domain with $i_\mathrm{max} = j_\mathrm{max} = 100$. Then, for ADI and ADOVI, in each time step 101 tridiagonal SLEs with 101 unknowns each must be solved, which can easily and efficiently be done by Gaussian elimination for tridiagonal matrices. By contrast, the implicit and OVI schemes lead to one SLE with $101^2 = 10{,}201$ unknowns, which corresponds to a matrix with $10{,}201^2 = 104{,}060{,}401$ entries, most of which are equal to zero ("sparse matrix"). Here, great care must be taken to apply a computationally manageable and efficient solution technique.

In SICOPOLIS, the matrix is stored in row-indexed sparse storage mode, which requires storage of only about twice the number of nonzero elements [19]. The SLE is then solved with the successive over-relaxation method (SOR, e.g., Törnig and Spellucci [20]), an iterative scheme which does not affect the matrix elements themselves, but is based on matrix-vector multiplications for which the row-indexed sparse storage mode is optimized. Therefore, the SOR method works very fast and efficiently for our problem. The convergence criterion is chosen as

$$\max\left\{ \left(h_{i,j}^{n+1}\right)_{s+1} - \left(h_{i,j}^{n+1}\right)_{s} \right\}_{\substack{i=0\,(1)\,i_{\max} \\ j=0\,(1)\,j_{\max}}} < \varepsilon_{\mathrm{SOR}}, \quad \varepsilon_{\mathrm{SOR}} = 10^{-5}\,\overline{a_{\mathrm{s}}^{+}}\,\Delta t, \tag{19}$$

where the index s counts the SOR iterations for the unknowns $h_{i,j}^{n+1}$, and $\overline{a_{\mathrm{s}}^{+}}$ is the spatial mean of the present accumulation rate of the simulated ice sheet. Due to the nonsymmetric matrix, stability is not guaranteed for over-relaxation parameters $\omega_{\mathrm{SOR}} > 1$, so that we use $\omega_{\mathrm{SOR}} = 1$ (also known as "Gauss–Seidel scheme").

In principle, it is also possible to evaluate the diffusivities D_{h} in (18) at the new time level t^{n+1}, which leads to a nonlinear algebraic equation for the unknowns $h_{i,j}^{n+1}$. This is not pursued here, but was discussed by Hindmarsh and Payne [11] for the purely dynamic problem (isothermal conditions).

4. SIMULATIONS FOR THE EISMINT PHASE 2 SIMPLIFIED GEOMETRY

4.1. Set-up

Within the European Ice Sheet Modelling Initiative (EISMINT), a program funded by the European Science Foundation (ESF), intercomparisons of thermomechanical ice-sheet models operated by research groups all over the world were carried out. One of these intercomparison studies were the EISMINT phase 2 simplified geometry experiments reported by Payne *et al.* [18]. The model domain of these experiments is a flat square bedrock of size $1500 \times 1500\ \mathrm{km}^2$. Axisymmetric boundary conditions with respect to the center of the square are prescribed for snowfall, surface melting, and surface temperature, which mimic roughly the conditions for the present Greenland ice sheet. Here, only "Experiment A" will be considered, which is a simulation into steady state over 200 kyr with time-independent boundary conditions, starting from ice-free initial conditions (for details, see [18]). Basal sliding is not accounted for, so that only internal deformation contributes to the ice flow, and the bedrock position is held fixed (no isostasy). For the horizontal plane, we apply two different grid spacings, the original fine grid with $\Delta x = \Delta y = 25\ \mathrm{km}$ (61×61 grid points), and a coarse grid with $\Delta x = \Delta y = 75\ \mathrm{km}$ (21×21 grid points). The vertical direction is discretized by 51 grid points in the cold-ice layer, 11 grid points in the temperate-ice layer (if existing; only relevant for the polythermal mode; see below), and 11 grid points in the lithosphere.

Unless stated otherwise, the simulations discussed below have been carried out in the "cold-ice mode." This means that the transition surface which separates cold and temperate ice is not monitored physically adequately by fulfilling Stefan-type conditions (Greve [6, 7]) and that the water-content equation is not solved in temperate-ice regions (conducting this is referred to as "polythermal mode"). Instead, the temperature equation is solved for the whole ice sheet, and temperatures exceeding pressure melting are artificially reset. This is done in order to achieve better comparability with other current ice-sheet models, which use

only the cold-ice mode. However, the performance of the model in the polythermal mode will also be reported briefly.

4.2. Stability and Accuracy

To assess the stability performance of the various marching schemes for the ice-thickness equation defined in Section 3, the maximum time steps Δt, $\widetilde{\Delta t}$ are determined for which stable integration of Experiment A can be achieved (only values $m \times 10^p$ yr with $m \in \{1, 2, 5\}$ and integer p tested). The results for EXPL, ADI, ADOVI ($w = 3$), IMPL, OVI ($w = 1.5$), and OVI ($w = 3$) are given in Table I together with corresponding CPU times on a PII 400 MHz LINUX PC (compilation with the NAGWare Fortran 95 compiler Release 4.1, optimization level O2).

Evidently, for the 25-km grid, the dynamic time step Δt varies by a factor 40 between the least stable scheme EXPL and the most stable schemes OVI ($w = 1.5$, $w = 3$), whereas the thermodynamic time step $\widetilde{\Delta t}$ is not affected. The variation in Δt is reflected in CPU times ranging from ca. three and a half hours (EXPL) to one-fourth hour (OVI, $w = 1.5$, $w = 3$). The stabilizing effect of over-weighing the implicit contribution in OVI and ADOVI is clearly visible. Δt can be increased by a factor of 4 in OVI ($w = 1.5$, $w = 3$) compared to IMPL, and still by a factor of 2 in ADOVI ($w = 3$) compared to ADI. However, unconditional stability, which was proven by Hindmarsh [10] for OVI with $w \geq n/2$ (=1.5) and isothermal conditions, does not hold in our thermomechanically coupled situation.

By contrast, for the coarse 75-km grid, all schemes except EXPL can be run with the same time steps. Apparently, in this case the limiting factor for stability arises from the thermodynamic model components, of which the numerical solution has been left unchanged in our study.

The accuracy of the results is assessed by comparison with a reference run conducted with the 25-km grid, the most natural scheme EXPL and the very small time steps $\Delta t = 1$ yr, $\widetilde{\Delta t} = 10$ yr. This reference run yields an ice sheet with volume $V_{\text{ref}} = 2.079 \times 10^6$ km^3, basal area $A_{\text{ref}} = 1.031 \times 10^6$ km^2, maximum thickness $H_{\text{ref}} = 3.655$ km, and melt fraction (ratio of basal area at pressure melting to total basal area) $f_{\text{ref}} = 0.699$. The predicted surface-elevation and ice-thickness distributions (identical due to the flat bedrock) are displayed in Fig. 4, and Fig. 5 shows the velocity and temperature fields in a transect across the center. The expected ice flow toward the margin, driven by the surface gradient, comes out very nicely, and the typical densification of temperature contours close to the base due to advective transport of cold ice downward is clearly visible as well.

Let V, A, H, and f be the corresponding results of an arbitrary simulation, then relative errors are defined as

$$r_V = \frac{V - V_{\text{ref}}}{V_{\text{ref}}}, \quad r_A = \frac{A - A_{\text{ref}}}{A_{\text{ref}}}, \quad r_H = \frac{H - H_{\text{ref}}}{H_{\text{ref}}}, \quad r_f = \frac{f - f_{\text{ref}}}{f_{\text{ref}}}. \tag{20}$$

These errors are listed in Table I for EXPL, ADI, ADOVI ($w = 3$), IMPL, OVI ($w = 1.5$), and OVI ($w = 3$). For the 25-km grid, the volume and maximum-thickness errors, r_V and r_H, show a slight tendency to increase with increasing time step Δt for the different schemes. In contrast, the basal area is computed without any error for all schemes. This is so because it is determined mainly by the surface mass balance (snowfall, melting), the parameterization of which does not depend on the numerical scheme, and only to a lesser extent by the internal dynamics. The error of the melt fraction r_f, which is dominated by thermodynamic effects,

TABLE I
Stability Performance (Maximum Time Steps Δt, $\widetilde{\Delta t}$), CPU Time (on a PII 400 MHz LINUX PC), and Accuracy (Relative Errors r_V, r_A, r_H, r_f)

Scheme	Max. $\Delta t/\widetilde{\Delta t}$ [yr]	CPU time [min]	r_V [%]	r_A [%]	r_H [%]	r_f [%]
Grid spacing 25 km:						
EXPL	5/200	215.6	−1.67	0	−0.67	−2.08
ADI	10/200	123.0	−1.68	0	−0.67	−1.74
ADOVI ($w = 3$)	20/200	65.9	−1.72	0	−0.68	−0.69
IMPL	50/200	32.8	−1.75	0	−0.68	−1.39
OVI ($w = 1.5$)	200/200	14.4	−2.05	0	−0.72	−2.61
OVI ($w = 3$)	200/200	15.3	−2.34	0	−0.77	−1.91
Grid spacing 75 km:						
EXPL	50/200	3.33	−6.77	−3.40	−1.90	0.29
ADI	200/200	1.47	−7.17	−3.40	−2.13	6.76
ADOVI ($w = 3$)	200/200	1.51	−7.61	−3.40	−2.23	3.52
IMPL	200/200	1.53	−7.38	−3.40	−2.12	4.32
OVI ($w = 1.5$)	200/200	1.56	−7.81	−3.40	−2.69	3.52
OVI ($w = 3$)	200/200	1.54	−8.38	−3.40	−2.82	3.52

Note. Different solution schemes of the ice-thickness equation for the steady-state EISMINT phase 2 simplified geometry simulations according to (18) are compared.

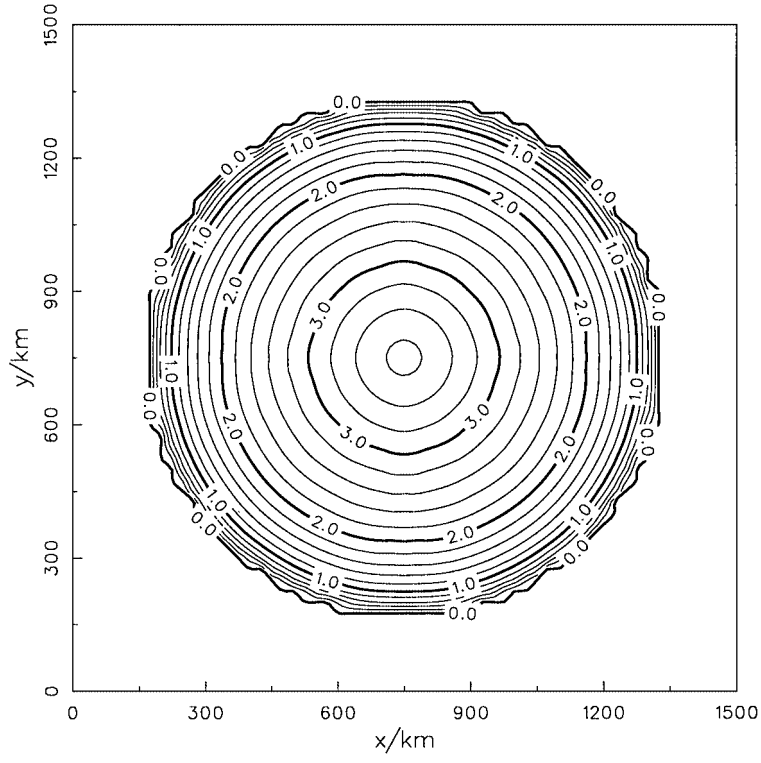

FIG. 4. Surface elevation and ice thickness (identical due to the flat bedrock) of the EISMINT phase 2 simplified geometry reference run. Labels in km, contour spacing 200 m.

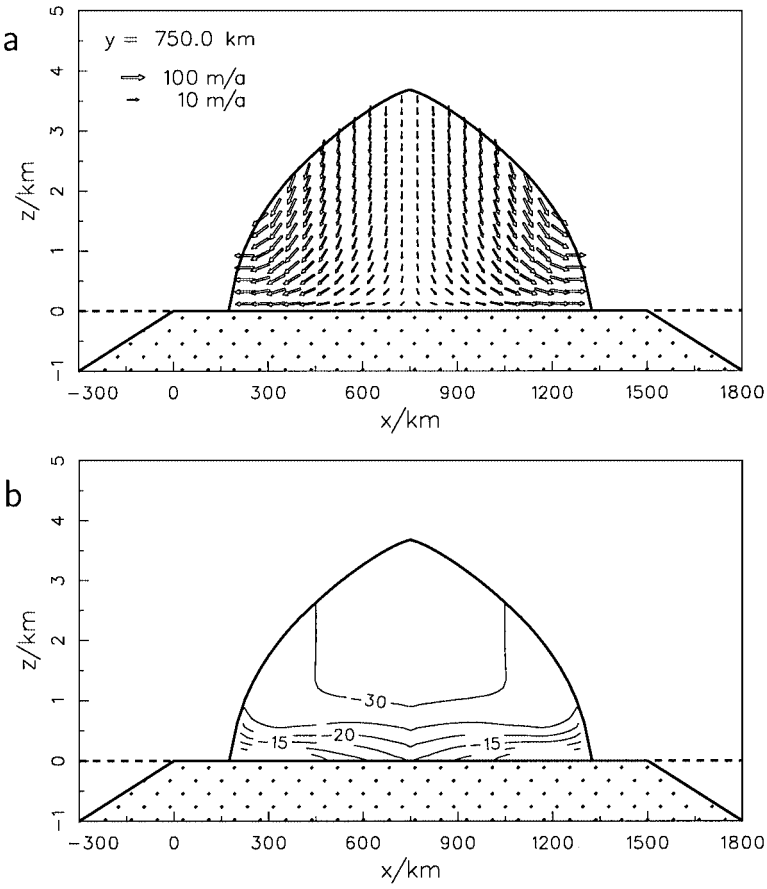

FIG. 5. Transect across the center of the ice sheet of the EISMINT phase 2 simplified geometry reference run. (a) flow velocity, (b) homologous temperature (temperature relative to pressure melting; labels in °C, contour spacing 5°C).

is apparently not correlated to Δt. All occurring errors are less than 3% and therefore small. Hence, all tested schemes produce reasonably accurate results for the simple, academic set-up considered here, so that the stability limits of the fastest schemes OVI ($w = 1.5$, $w = 3$) can be fully made use of.

For the 75-km grid, all errors are naturally larger. The volume and maximum-thickness errors, r_V and r_H, show again a slight increase from EXPL to OVI ($w = 3$). As the time steps Δt are the same for all schemes except EXPL, this increase cannot be attributed to increasing time steps, but is an intrinsic consequence of the schemes themselves. In particular, it can be clearly seen that over-weighing the implicit contributions in OVI and ADOVI decreases the accuracy of the computed ice volumes and maximum thicknesses compared to IMPL and ADI. Like for the 25-km grid, the results for the basal area are unaffected by the different schemes, and the errors of the melt fraction do not show a clear trend.

The simulation with the 25-km grid and OVI ($w = 3$) has been re-run in the polythermal mode. This does not affect the maximum time steps; $\Delta t = 200$ years, $\widetilde{\Delta t} = 200$ years still gives a stable integration. Nevertheless, the CPU time rises to 41.7 min, almost three times as much as in the cold-ice mode (Table I). This is mainly due to the fact that the

transition surface between cold and temperate ice is determined iteratively by a trial-and-error procedure, which requires several recomputations of the temperature and water content during a single iteration step [6, 8]. The results for V, A, H, and f are within 2% of those obtained in the cold-ice mode. However, the computed volumes of the near-basal temperate-ice layer differ strongly, they are 1.669×10^4 km^3 in the polythermal mode and 6.728×10^4 km^3 in the cold-ice mode. This tendency of the cold-ice mode to overestimate temperate-ice volumes was already reported and discussed by Greve [8]. Nonetheless, the emphasis of our study is on the cold-ice mode, because most of the other current ice-sheet models operate in this mode only.

5. SIMULATIONS FOR THE NORTHERN HEMISPHERE

5.1. Set-up

As an application of the ice-sheet model SICOPOLIS to a real problem, now paleoclimatic simulations for the entire northern hemisphere prone to glaciation (North America, Eurasia, Greenland, Tibet, Alps) are discussed. The set-up follows closely the one described by Greve *et al.* [9], so only the most important points are repeated here.

The surface of the northern hemisphere is projected to a polar stereographic map with standard parallel at 71°N. In the stereographic plane, the model domain is a 12480×12480 km^2 square centered at the north pole. This domain includes the whole area north of 40°N and extends beyond 30°N in the Tibet/Himalaya region. The distortion which arises from the projection is accounted for by introducing the corresponding components of the (orthogonal) metric tensor in all terms with horizontal derivatives in the model equations. Two different grid spacings are applied for the stereographic plane, a fine grid with $\Delta x = \Delta y = 80$ km (157×157 grid points), and a coarse grid with $\Delta x = \Delta y = 160$ km (79×79 grid points). In the vertical, 21 grid points are used in the cold-ice layer, 11 grid points in the temperate-ice layer (only polythermal mode), and 11 grid points in the lithosphere. Again, if not stated otherwise, the simpler cold-ice mode is applied for comparability.

The simulations cover the period from 250 kyr BP (before present) until today, that is, they run over two glacial/interglacial cycles. Present snowfall and surface-temperature distributions are derived from data by Jaeger [15] and ECMWF (European Centre for Medium-Range Weather Forecast, Reading, U.K., www.ecmwf.int), respectively. For past times, the 250-kyr δ^{18}O record of the GRIP ice core (Fig. 6; Dansgaard *et al.* [4]), which

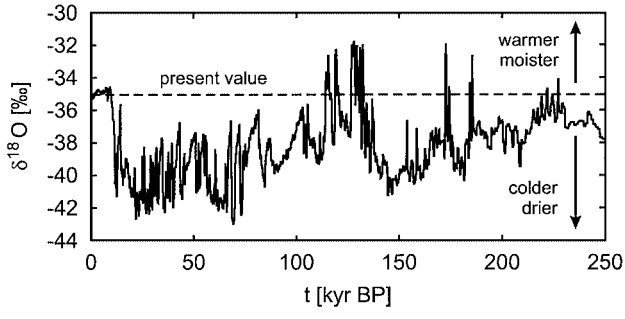

FIG. 6. δ^{18}O record of the GRIP ice core [4]. The dashed line indicates the present level. More positive values correspond to warmer and moister (more precipitation) conditions, more negative values to colder and drier (less precipitation) ones.

is a proxy for the surface-temperature and snowfall history in central Greenland, is used to offset these distributions without changing their spatial pattern. The latter procedure is only a coarse approximation to real conditions, as changes in atmospheric and oceanic circulations are likely to influence the spatial distributions of these climatic input quantities. Surface melting is parameterized by a simple degree-day approach. The simulations start from arbitrarily chosen ice-free conditions at 250 kyr BP, so that the first ca. 50 kyr of model time are required for spin-up, until the influence of the initial conditions has faded.

In contrast to the EISMINT simulations of Section 4, isostatic bedrock displacement is included, and basal sliding appears in regions where the temperature of the basal ice is at pressure melting. These processes are closer to reality, and at the same time represent an additional challenge to the stability of the numerical schemes.

5.2. Stability and Accuracy

The same investigation on stability as described above (Section 4.2) for the EISMINT simulations has been carried out for the paleoclimatic northern hemisphere simulations. The maximum time-steps and CPU times for the schemes EXPL, ADI, ADOVI ($w = 3$), IMPL, OVI ($w = 1.5$), and OVI ($w = 3$) are listed in Table II.

Again, for the fine grid (spacing 80 km), the dynamic time step Δt increases greatly (by a factor of 20) from EXPL to OVI, whereas the thermodynamic time step $\widetilde{\Delta t}$ remains constant. It is remarkable that IMPL is stable with the same time steps as OVI ($w = 1.5$, $w = 3$) and even needs less CPU time. The latter is due to the fact that IMPL requires fewer iterations for fulfilling the convergence criterion (19) of the SOR solver. By contrast, ADOVI ($w = 3$) allows a twice as large Δt than ADI, which is the same stabilising effect as in the EISMINT simulations.

TABLE II

Stability Performance (Maximum Time Steps Δt, $\widetilde{\Delta t}$), CPU Time (on a PII 400 MHz LINUX PC), and Accuracy (Relative Errors r_V, r_A, r_H, r_f) at the Last Glacial Maximum, t = 18 kyr BP

Scheme	Max. $\Delta t/\widetilde{\Delta t}$ [yr]	CPU time [hr]	r_V [%]	r_A [%]	r_H [%]	r_f [%]
Grid spacing 80 km:						
EXPL	5/100	18.34	−0.16	0.23	−0.20	1.70
ADI	10/100	10.35	−0.27	0.09	−0.22	1.15
ADOVI ($w = 3$)	20/100	5.35	−0.77	−0.25	−0.36	0.05
IMPL	100/100	1.77	−1.86	−1.33	−0.33	−3.15
OVI ($w = 1.5$)	100/100	1.88	−4.91	−3.05	−0.50	−8.33
OVI ($w = 3$)	100/100	2.11	−7.06	−4.36	−0.76	−12.11
Grid spacing 160 km:						
EXPL	10/100	2.76	−4.45	−1.73	−2.05	13.74
ADI	50/200	0.57	−6.55	−3.00	−2.11	12.51
ADOVI ($w = 3$)	100/200	0.30	−11.86	−6.57	−2.91	2.18
IMPL	200/200	0.20	−10.36	−5.98	−2.62	1.43
OVI ($w = 1.5$)	200/200	0.20	−11.21	−6.44	−2.55	−2.60
OVI ($w = 3$)	200/200	0.20	−14.34	−7.83	−2.45	−9.01

Note. Different solution schemes of the ice-thickness equation for the transient northern hemisphere simulations according to (18) are compared.

The situation is very similar for the coarse grid (spacing 160 km). The dynamic time step Δt of scheme EXPL is smaller by a factor of 20 than the one of schemes IMPL and OVI ($w = 1.5$, $w = 3$). ADI and ADOVI ($w = 3$) differ by a factor of 2, whereas IMPL and OVI ($w = 1.5$, $w = 3$) can be run with the same time steps. In contrast to the 80-km grid, scheme EXPL requires a smaller thermodynamic time step $\widetilde{\Delta t}$ than the other schemes.

As above (Section 4.2), a run with the fine grid (spacing 80 km), the scheme EXPL, and the very small time steps $\Delta t = 1$ year, $\widetilde{\Delta t} = 10$ year have been carried out to obtain a reference result against which the results of the several runs can be checked. For the Last Glacial Maximum (LGM) at $t = 18$ kyr BP this yields an extended glaciation with volume $V_{\mathrm{ref}}^{\mathrm{LGM}} = 66.87 \times 10^6$ km^3, basal area $A_{\mathrm{ref}}^{\mathrm{LGM}} = 32.70 \times 10^6$ km^2, maximum thickness $H_{\mathrm{ref}}^{\mathrm{LGM}} = 4.162$ km, and melt fraction $f_{\mathrm{ref}}^{\mathrm{LGM}} = 0.400$, which covers large parts of north America, Greenland, Scandinavia, Eurasia, and Tibet. At present, apart from some ice remnants in the Russian Arctic and Tibet, only the Greenland ice sheet remains, so that $V_{\mathrm{ref}}^{\mathrm{present}} = 5.584 \times 10^6$ km^3, $A_{\mathrm{ref}}^{\mathrm{present}} = 3.483 \times 10^6$ km^2, $H_{\mathrm{ref}}^{\mathrm{present}} = 3.496$ km, and $f_{\mathrm{ref}}^{\mathrm{present}} = 0.386$ (Fig. 7).

The relative errors r_V, r_A, r_H, and r_f [Eq. (20)] of the several schemes are given in Table II for the LGM time-slice where the ice volume takes a maximum. For the 80-km grid, all errors essentially increase with increasing time step Δt for the different schemes. Compared to the EISMINT simulations, the variability among the schemes is much larger, and a distinct discontinuity occurs between IMPL and OVI ($w = 1.5$), even though these schemes have been run with the same time steps. Evidently, the over-weighing procedure worsens the accuracy not only due to larger time-steps, but also due to the method itself, as we have already seen for the EISMINT simulations. OVI ($w = 1.5$) and OVI ($w = 3$) show volume errors of ca. 5 and 7%, respectively, compared to less than 2% for the other schemes, so that the accuracy of the OVI simulations is severely limited. The best compromise between stability and accuracy is clearly the simulation with IMPL. For the 160-km grid, the errors show the same increasing trend from EXPL to OVI ($w = 3$), but on a generally higher level due to the lower spatial resolution.

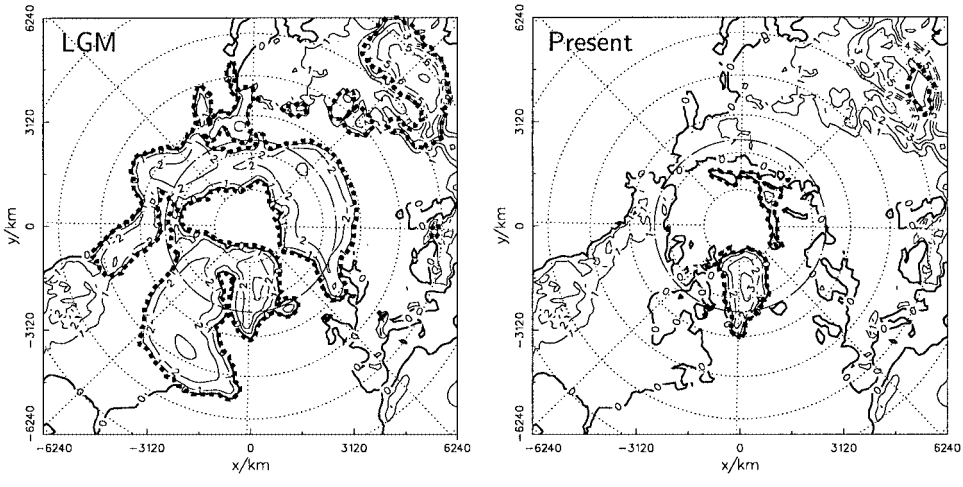

FIG. 7. Surface elevation of the northern-hemisphere reference run at the Last Glacial Maximum ($t =$ 18 kyr BP) and the present. Labels in km above mean present sea level, contour spacing 1 km, latitude circles spaced by 10°, longitude lines by 45°. Dashed heavy lines indicate ice margins.

TABLE III
CPU Time (on a PII 400 MHz LINUX PC) and Accuracy (Relative Errors r_V, r_A, r_H, r_f) at the Last Glacial Maximum, t = 18 kyr BP

Scheme	CPU time [hr]	r_V [%]	r_A [%]	r_H [%]	r_f [%]
EXPL	18.34	−0.16	0.23	−0.20	1.70
ADI	19.93	−0.22	0.14	−0.23	1.30
ADOVI ($w = 3$)	20.37	−0.35	0.05	−0.27	1.08
IMPL	20.68	−0.29	0.13	−0.24	1.25
OVI ($w = 1.5$)	22.20	−0.31	0.11	−0.27	0.95
OVI ($w = 3$)	20.99	−0.60	−0.16	−0.33	0.75

Note. Different solution schemes of the ice-thickness equation for the transient northern hemisphere simulations according to (18) are compared. Grid spacing is 80 km, maximum time steps of scheme EXPL ($\Delta t = 5$ yr, $\widetilde{\Delta t} = 100$ yr; see Table II) applied.

It is interesting to compare the EISMINT simulations for the 75-km grid with the northern-hemisphere simulations for the similar 80-km grid. We have seen above that for the academic EISMINT problem with the 75-km grid stability is no longer limited by the ice-thickness equation, so that all schemes (except EXPL) can be run with the same time steps. By contrast, the similar 80-km grid for the "real-world" northern-hemisphere problem with uneven bedrock topography, isostasy, time-dependent boundary conditions and basal sliding leads to a very strong dependence of numerical stability on the applied scheme for the ice-thickness equation. Therefore, the stability of the numerical solution of the ice-thickness equation is strongly affected by these real-world phenomena. Evidently, the thermodynamic part is less sensitive; the thermodynamic time step for the EISMINT problem is only twice as large (200 years) as the one for the northern-hemisphere problem (100 years).

In order to separate the impacts of different time steps and different numerical schemes on accuracy, the northern-hemisphere simulations on the 80-km grid have been repeated with fixed time steps $\Delta t = 5$ year, $\widetilde{\Delta t} = 100$ year (which are the maximum time steps for scheme EXPL). The resultant CPU times and relative errors are shown in Table III. The former vary only by ca. 20% among the different schemes, which demonstrates in particular the efficiency of the SOR solver for the very large and sparse SLEs of the schemes IMPL and OVI. The latter are generally small due to the small time steps, except for some values of r_f always less than 1%. The errors r_V and r_H, which are most directly influenced by the solution of the ice-thickness equation, increase in the order EXPL < ADI < IMPL < OVI ($w = 1.5$) < ADOVI ($w = 3$) < OVI ($w = 3$), which reflects the decreasing accuracy of the schemes. However, comparison with Table II shows that by far the larger part of the errors arises from the increasing time steps if the stability limits of the several schemes are fully made use of.

Re-running the simulation with the 80-km grid and the scheme OVI ($w = 3$) in the polythermal mode allows maximum time steps of $\Delta t = 20$ years, $\widetilde{\Delta t} = 20$ years, which is five times smaller than in the cold-ice mode (Table II), in strong contrast to the above findings for the EISMINT set-up where the maximum time steps remained unaffected. The corresponding CPU time is 9.59 h, ca. 4.5 times the CPU time required for the cold-ice mode. Apparently, the real-world problem de-stabilizes the polythermal mode to a much larger extent than the cold-ice mode. Comparison with a run in the cold-ice mode and the same settings [grid spacing 80 km, OVI ($w = 3$), $\Delta t = 20$ years, $\widetilde{\Delta t} = 20$ years] shows

again very similar results for the large-scale properties V, A, H, and f (differences $<0.5\%$ for the LGM and $<3\%$ for the present), whereas the volumes of the near-basal temperate-ice layer, which are of the order of 1% of the total ice volume, are larger by a factor 2.1 (LGM) and 3.7 (present) in the cold-ice mode.

6. CONCLUSION

The stability and accuracy of a variety of numerical solution schemes for the ice-thickness equation within the dynamic/thermodynamic ice-sheet model SICOPOLIS has been investigated for two different problems, a simple axi-symmetric steady-state ice sheet which rests on a flat bedrock ("EISMINT phase 2 simplified geometry experiment") and the time-dependent glaciation of the northern hemisphere from 250 kyr BP over two climatic cycles until today. As expected, the stability increases in the order EXPL < ADI < ADOVI < IMPL < OVI, maximum dynamic time steps Δt varying by up to a factor of 40 between the least and the most stable scheme. Correspondingly, CPU times can be reduced by up to a factor of 15. For the simple EISMINT problem, this is not accompanied by a significant decrease in accuracy, whereas for the "real-world" problem of paleo-glaciation of the northern hemisphere, which includes an uneven bedrock topography, isostasy, time-dependent boundary conditions, and basal sliding, the accuracy worsens distinctly when OVI is applied; here IMPL is the best compromise between stability (short computing time) and accuracy.

For the EISMINT problem, application of the polythermal mode has no effect on stability in case of the OVI scheme, and produces distinctly less near-basal temperate ice while leaving large-scale ice-sheet properties essentially unchanged. The latter holds also for the northern-hemisphere problem, whereas in this case the stability of the OVI scheme is significantly reduced.

ACKNOWLEDGMENTS

For the implementation of the implicit and over-implicit schemes, R.G. has greatly profited from discussions with T. Zwinger, P.-L. Forsström, J. Heikonen, V. Savolainen, and J. Ruokolainen during a visit at CSC–Scientific Computing Ltd., Espoo, Finland. We also express our gratitude to K. Hutter for reading and correcting an earlier version of the manuscript and R.C.A. Hindmarsh and two anonymous referees who helped considerably to improve the quality of this paper.

REFERENCES

1. A. Arakawa and V. R. Lamb, Computational design of the basic dynamical processes of the UCLA general circulation model, in *Methods in Computational Physics* **17**, edited by J. Chang (Academic Press, New York, 1977), pp. 173–265.
2. D. R. Baral, K. Hutter, and R. Greve, Asymptotic theories of large-scale motion, temperature and moisture distribution in land-based polythermal ice sheets. A critical review and new developments, *Appl. Mech. Rev.* **54**(3), 215 (2001).
3. R. Calov and K. Hutter, Large scale motion and temperature distributions in land-based ice shields; the Greenland Ice Sheet in response to various climatic scenarios, *Arch. Mech.* **49**(5), 919 (1997).
4. W. Dansgaard, S. J. Johnsen, H. B. Clausen, D. Dahl-Jensen, N. S. Gundestrup, C. U. Hammer, C. S. Hvidberg, J. P. Steffensen, A. E. Sveinbjörnsdottir, J. Jouzel, and G. Bond, Evidence for general instability of past climate from a 250-kyr ice-core record, *Nature* **364**, 218 (1993).

5. K. Fleming, P. Johnston, D. Zwartz, Y. Yokoyama, K. Lambeck, and J. Chappel, Refining the eustatic sea-level curve since the Last Glacial Maximum using far- and intermediate-field sites, *Earth Planet. Sci. Lett.* **163**, 327 (1998).
6. R. Greve, Thermomechanisches Verhalten polythermer Eisschilde-Theorie, Analytik, Numerik, Ph.D. thesis (Institut für Mechanik, Technische Hochschule Darmstadt, Germany, 1995). [Available from Shaker Verlag (Series Berichte aus der Geowissenschaft), Aachen, Germany.]
7. R. Greve, A continuum-mechanical formulation for shallow polythermal ice sheets, *Phil. Trans. R. Soc. Lond., Ser. A* **355**, 921 (1997).
8. R. Greve, Application of a polythermal three-dimensional ice sheet model to the Greenland Ice Sheet: Response to steady-state and transient climate scenarios, *J. Climate* **10**(5), 901 (1997).
9. R. Greve, K.-H. Wyrwoll, and A. Eisenhauer, Deglaciation of the Northern Hemisphere at the onset of the Eemian and Holocene, *Ann. Glaciol.* **28**, 1 (1999).
10. R. C. A. Hindmarsh, Notes on basic glaciological computational methods and algorithms, in *Continuum Mechanics and Applications in Geophysics and the Environment*, edited by B. Straughan, R. Greve, H. Ehrentraut, and Y. Wang (Springer-Verlag, Berlin, 2001), pp. 222–249.
11. R. C. A. Hindmarsh and A. J. Payne, Time-step limits for stable solutions of the ice-sheet equation, *Ann. Glaciol.* **23**, 74 (1996).
12. K. Hutter, *Theoretical Glaciology; Material Science of Ice and the Mechanics of Glaciers and Ice Sheets* (Reidel, Dordrecht, 1983).
13. K. Hutter, Thermo-mechanically coupled ice-sheet response—Cold, polythermal, temperate, *J. Glaciol.* **39**(131), 65 (1993).
14. P. Huybrechts, A. J. Payne, and the EISMINT Intercomparison Group, The EISMINT benchmarks for testing ice-sheet models, *Ann. Glaciol.* **23**, 1 (1996).
15. L. Jaeger, Monatskarten des Niederschlags für die ganze Erde, *Ber. Dtsch. Wetterdienstes* **139**, (1976).
16. L. W. Morland, Thermo-mechanical balances of ice sheet flows, *Geophys. Astrophys. Fluid Dyn.* **29**, 237 (1984).
17. W. S. B. Paterson, *The Physics of Glaciers*, 3rd ed. (Pergamon, Oxford, 1994).
18. A. J. Payne, P. Huybrechts, A. Abe-Ouchi, R. Calov, J. L. Fastook, R. Greve, S. J. Marshall, I. Marsiat, C. Ritz, L. Tarasov, and M. P. A. Thomassen, Results from the EISMINT model intercomparison: the effects of thermomechanical coupling, *J. Glaciol.* **46**(153), 227 (2000).
19. W. H. Press, S. A. Teukolsky, W. T. Vetterling, and B. P. Flannery, *Numerical Recipes in Fortran 77*. 2nd ed. (Cambridge Univ. Press, Cambridge, UK, 1996).
20. W. Törnig and P. Spellucci, *Numerische Mathematik für Ingenieure und Physiker. Band 1: Numerische Methoden der Algebra* (Zweite Auflage. Springer-Verlag, Berlin, 1988).